An AC−STM Study of Mineral Sulfides and the Tip Induced Oxidation of PbS†

A. Szuchmacher Blum,*,‡ Adam J. D. Schafer,§ and Thomas Engel

Department of Chemistry, University of Washington, Box 351700, Seattle, Washington 98195

Received: March 5, 2002; In Final Form: June 10, 2002

Three different mineral sulfide surfaces were studied using an alternating current scanning tunneling microscope (AC−STM). This technique, which is based on an applied alternating current bias voltage, is able to measure both conducting and insulating surfaces with the resolution of an STM. By comparing the three sulfides (CuS, MoS_2, and PbS) with H−Si(111), we could examine the third harmonic generation mechanism on semiconductor surfaces. In addition, the tip-induced oxidation of PbS was observed, starting from a clean PbS surface until an insulating oxide film covered the surface. The reaction was observed with real-time imaging, allowing both the nucleation and growth of an insulating film to be observed without loss of resolution due to insufficient DC tunneling current.

Introduction

Scanning tunneling microscopy (STM) has proved to be a valuable method to investigate the structure and properties of surfaces at an atomic level.[1] Although the tunneling current used under normal operating conditions in an STM is small, the current density in the filament between the tip and surface is on the order of 10^6 A cm^{-2}. This limits the applicability of STM to conductive surfaces. The development of alternating current STM (AC−STM)[2] has extended the applicability of tunneling microscopy to materials with low conductivity.

With this technique, an alternating current driving voltage is applied to an STM junction. Nonlinearities in the junction produce higher harmonics in the tunneling current, which are then used for feedback control and imaging. The third harmonic has proven particularly useful for imaging studies using AC−STM. Prior workers in the field have demonstrated that the electronic properties of the sample are very important in establishing how successful the AC−STM will be for high-resolution imaging of a given surface. In previous studies, examinations of the mechanism of third harmonic generation have been done on graphite (HOPG),[3,4] two different semiconductors (CuO and WSe_2),[2,3] and an insulating film (SiO_2).[5,6] Thus far, two different potential third harmonic generation mechanisms have been demonstrated, only one of which yields a signal that is exponentially dependent on the distance between tip and sample, and is thus suitable for atomic resolution imaging.

In a series of experiments on graphite, the third harmonic signal was demonstrated to be proportional to the second derivative of the DC tunneling current with respect to the voltage.[3,4] As a nonlinear function of the tunneling current, this third harmonic signal has the same exponential gap size vs signal profile as for standard tunneling experiments.[7] As a result, several groups have been able to achieve lateral atomic resolution on graphite with the AC−STM.[4,8,9] Furthermore, in measurements of the signal as a function of distance, both the third harmonic and the DC tunneling current disappear within a few nm from the surface, as is expected for purely tunneling phenomena.[7]

In contrast, large third harmonic signals have been measured at distances up to 100 nm from the sample on WSe_2.[2,3] Since tunneling currents decay exponentially, these measurements cannot be due to electron tunneling. More likely, the measured third harmonic signal arises from a large displacement current that dominates the measurement. In addition, the third harmonic signal has been demonstrated to be proportional to the calculated second derivative of the capacitance with respect to the voltage.[3] Seifert attributes these observations to the voltage-dependent capacitance between the space-charge region immediately below the surface and the semiconductor surface, which depends on the bias voltage as $(\Phi - V)^{-1/2}$ where Φ is the work function and V is the applied voltage. In this model, the overall gap capacitance has a nonlinear dependence on the voltage, producing the observed higher harmonics.[3] Similarly, in measurements on the only insulating system described in detail (SiO_2/Si), the capacitive mechanism was found to be the dominant source of higher harmonics. In these experiments, a 10 nm SiO_2 film was grown on a clean, freshly etched Si surface via chemical oxidation. Several measurements demonstrate that the third harmonic signal on this sample is proportional to the second derivative of the capacitance with respect to the voltage,[5,6] as observed on WSe_2. In all of these studies where an appreciable third harmonic signal has been observed for tip−surface distances well in excess of 1.0 nm, topographical information at the atomic scale, such as steps and terraces, has not been observed.

In addition, there is a third possibility that has not been considered in the literature to date, namely, that both capacitance and tunneling can be important in producing third harmonic signal in some materials. For example, Kochanski shows this type of behavior on CuO. A plot of the third harmonic signal as a function of the tip−sample separation shows a strong third harmonic signal that extends from the surface to 75 nm.[2] The extent of this signal is indicative of capacitive effects, because the signal is still measurable beyond the range of electron tunneling. However, when the tip reaches DC tunneling range (at about 1 to 0.5 nm from the surface), there is a sharp increase in the third harmonic signal. Kochanski attributes this increase

† Part of the special issue "John C. Tully Festschrift."

* Corresponding author. E-mail: amyblum@cbmse.nrl.navy.mil.

‡ Current address: Naval Research Laboratory, Center for Biomolecular Science and Engineering, 4555 Overlook Avenue SW, Washington, DC 20375.

§ Current address: Intel Corporation, 5200 N. E. Elam Young Parkway, Hillsboro, OR 97124.

10.1021/jp020621+ CCC: $22.00 © 2002 American Chemical Society
Published on Web 07/20/2002

in third harmonic signal to AC tunneling.[2] Thus, on CuO, the dominant mechanism of third harmonic generation depends on how far the tip is from the surface, since apparently more than one harmonic generation mechanism is important.

Since so few studies have been done on different materials, it is difficult to know if there is any way to predict how third harmonics will be generated on a given surface and if AC−STM can be used to obtain topographical information at an atomic level. Previous workers have assumed that data for WSe_2 could be generalized to all semiconductors,[4] but the measurements described below demonstrate that this is not the case. In this paper, we present studies of the third harmonic signal generated on three different layered sulfides with varying band gaps, as well as on both oxidized and hydrogen-terminated silicon samples, in an attempt to determine the dominant type of nonlinearity present for each sample and to determine if atomic level structural information can be obtained using AC−STM. Using this information to aid in interpreting the data, we present a more detailed study of the tip-induced oxidation of the PbS surface.

Experimental Methods

Experiments were carried out using an AC−STM described below. The microscope was mounted in a glovebox that was filled with high purity nitrogen gas. Samples were introduced into the glovebox through a differentially pumped loadlock. All sample preparation was done under ambient conditions. For samples that oxidize in air, such as covellite (CuS) and galena (PbS), both sides of the crystal were cleaved before the samples were mounted, to ensure good ohmic contact. The samples were attached to the sample holder using conductive silver paste (Ted Pella). As soon as the samples were mounted, they were cleaned with pressurized dry nitrogen to remove particulates left behind by the cleaving process, then put into a dry nitrogen environment to slow oxidation of the newly exposed surface. Samples were held in the glovebox for 30−60 min prior to use.

The CuS and molybdenite (MoS_2) samples used for this study were obtained from Dr. Kevin Rosso at Pacific Northwest National Laboratory. The CuS was cleaved with a razor blade prior to use, while the MoS_2 was cleaved with Scotch tape. The PbS samples used for these experiments were borrowed from the University of Washington Department of Geology. The samples were naturally occurring galena crystals from Montana. The PbS samples were cleaved with a hammer and a razor blade prior to each use.

The silicon(111) samples were all cut from one phosphorus-doped n-type wafer (Mitsubishi Silicon America) with a miscut angle of $<1°$ and a resistivity of 2−8 Ωcm. Hydrogen-terminated samples were prepared via chemical etching as follows. Freshly cut samples were held vertically in a Teflon holder. The samples were rinsed with Millipore water (resistivity <15 MΩ), then cleaned in a solution of 4:1:1 water/H_2O_2/NH_4OH for 10 min at 80 °C. The H_2O_2 was electronics grade from J. T. Baker. The NH_4OH was reagent grade from Fischer. All chemicals were used as received, without further purification. Next, the samples were etched in buffered oxide etch (BOE, Transene), a concentrated buffered HF solution, for 3 min to remove the native oxide and upper layers of silicon. Samples were then reoxidized in 4:1:1 water/H_2O_2/NH_4OH solution at 80 °C for 10 min. After reoxidation, samples were again etched in BOE for 3 min. After the etching, samples were reoxidized a final time in 4:1:1 water/H_2O_2/NH_4OH. Final sample morphology was determined by hydrogen termination in electronics grade NH_4F (Transene) for 30 min. After etching, samples were briefly rinsed in Millipore water and then blown dry in nitrogen. Finally, samples were mounted and put into the glovebox.

Oxidized silicon(111) samples were prepared in a UHV system by Steve Moskowitz. Samples were cleaned via resistive heating, keeping the pressure below 10^{-8} Torr to prevent contamination. Once cleaned, the Si(111) samples were vented to pure oxygen to produce a native oxide layer on the surface. AFM measurements verified that the oxidized Si samples prepared in this way exhibited the expected step and terrace structure.

For all of the following measurements 90−10 platinum−iridium wire tips were used. For current vs voltage curves, commercially available (TopoMetrix) tips made from cut wire were used. A fresh tip was used for each measurement in order to keep the tips as sharp and uncontaminated as possible. For the AC−STM experiments, 0.002″ wire was cut with scissors prior to each experiment.

The STM and AC−STM images were taken with the instrument described below. For STM feedback imaging, the DC bias and tunneling varied, depending on the sample. The AC bias was 1.29 V_{p-p}. The measured AC signal varied, depending on the sample. For AC−STM feedback imaging, the DC bias was 0 V, unless otherwise specified. The AC bias was 1.29 V_{p-p}, with a setpoint of −61 dBm. At least 5 dBm above the noise floor (−76 dBm) is required for stable AC feedback imaging. All image analysis was done in Image SXM, a free modification of NIH−Image by Dr. Steve Barrett.

The AC−STM was designed and built in house, based on the microscope of Michel and co-workers.[7] The AC−STM consists of an STM head built into a rectangular microwave resonant cavity. Coupling is achieved through a probe input (the sample) and an antennae output (a simple wire loop) connected to the cavity with standard rigid coaxial cables. The microwave cavity is set to resonate at 2.36 GHz, a frequency range demonstrated to be useful by previous workers.[7,9] The AC signal is read from a spectrum analyzer into a PC for image display and processing. For DC STM, a bias voltage between −10 and 10 V is applied at the tip, while tunneling current is read out from the sample. AC and DC images can be acquired simultaneously.

Current vs voltage curves for these samples were measured on a commercially available TopoMetrix Explorer STM. Measurements were made both in a dry nitrogen environment and under ambient conditions. There was no statistically significant difference between measurements in the two environments. The I/V data were used to provide surface density of states (DOS) and band gap information about the samples used for the AC−STM study. Data were taken as the average of five measurements, with 300 data points between −2 and 2 V. Note that the AC−STM applies the DC bias to the sample, while the TopoMetrix instrument applies the DC bias to the tip. Thus, the relevant TopoMetrix data are opposite in sign to the data from the AC−STM. Analysis was done with the TopoMetrix software and with Microcal Origin 6.0. The DOS as a function of the applied voltage was calculated using the observation that in the low bias limit, a plot of $(dI/dV)/(I/V)$ represents a convolution of states on the tip and sample.[10] For a metal−semiconductor system, because the metal LDOS can typically be approximated as constant, features in the LDOS are here assumed to be dominated by the states of the semiconductor.

AFM measurements were taken on a Digital Instruments Nanoscope III instrument. The images were taken in tapping mode, with Digital Instruments TESP tips. Measurements were made under ambient conditions.

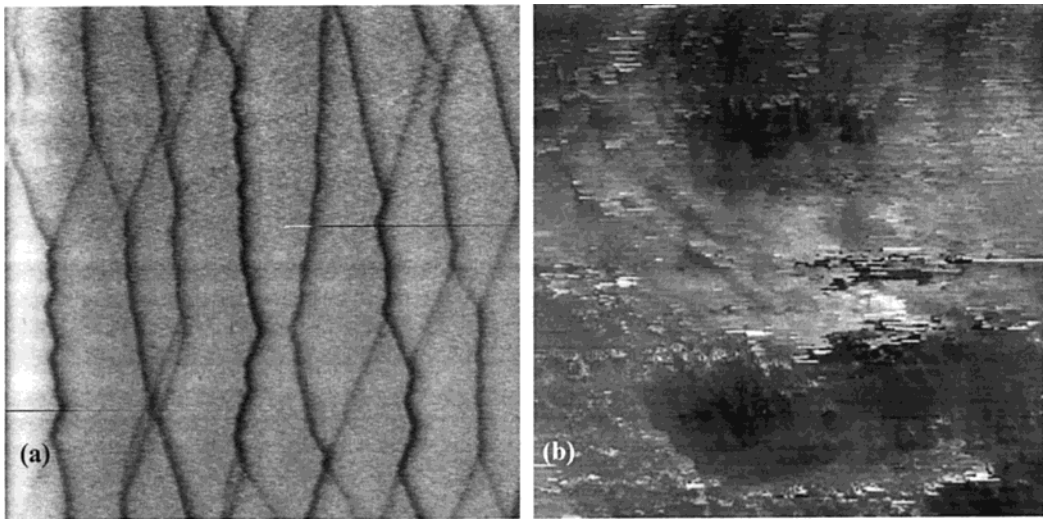

Figure 1. (a) 900 nm × 900 nm tapping mode AFM image. Average step size is 0.33 nm, which corresponds to a single atomic step. Scale, black to white is 0 to 2.0 nm. (b) 300 nm × 300 nm height image, taken with AC feedback control. Scale, black to white 0 to 22.08 nm. AC bias = 1.29 V_{p-p}. AC set point −61 dBm. Images taken on the same surface at different points.

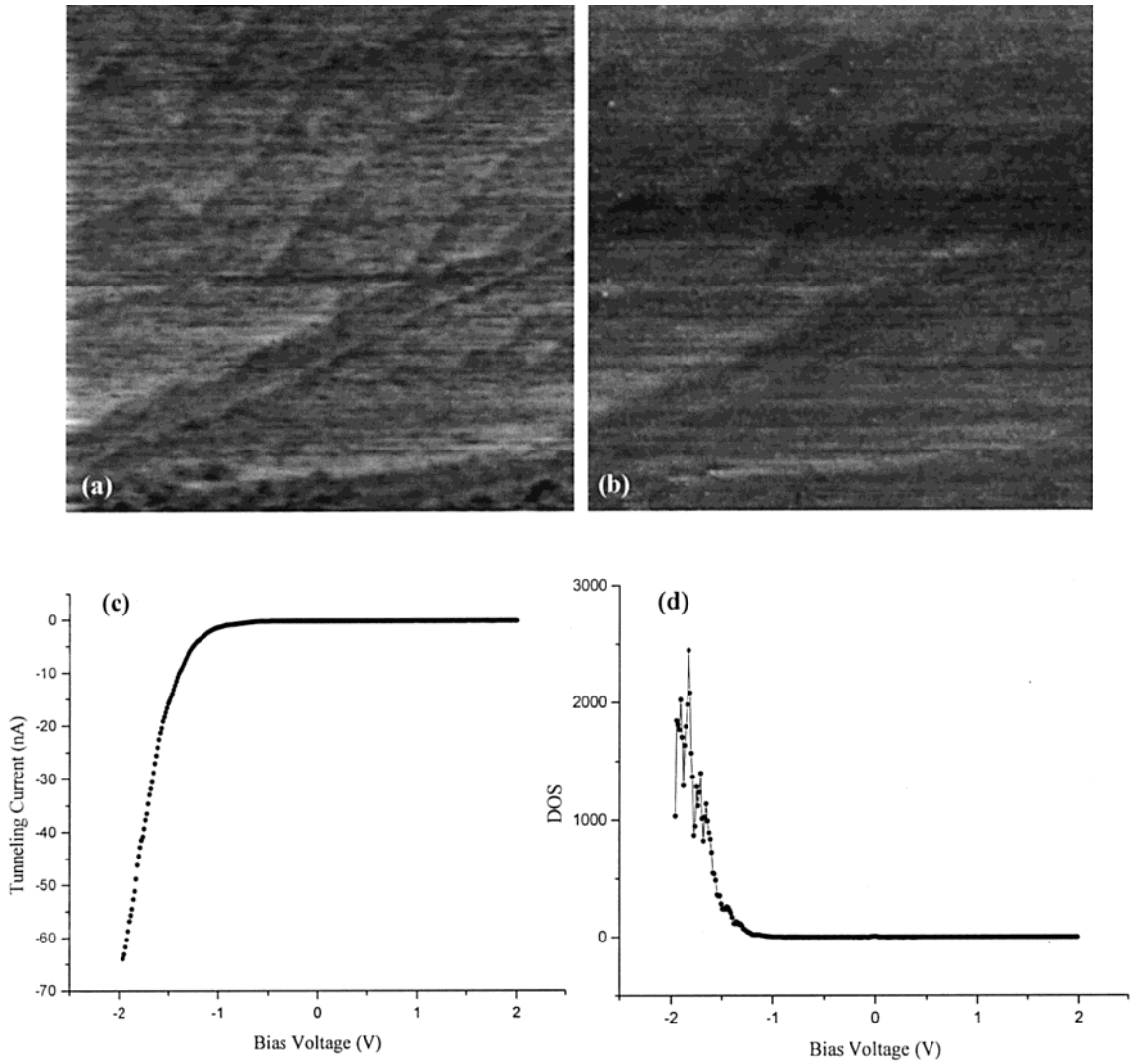

Figure 2. 300 nm × 300 nm. (a) DC height image and (b) TH signal image of H−Si(111), taken with DC feedback. DC bias = 1.5 V, I_t = 0.1 nA. AC bias = 1.29 V_{p-p}. Left scale, black to white, 0 to 14.22 nm. (c) Tunneling current and (d) DOS vs applied bias for H−Si(111). Unusual shape of curve due to saturation of surface states by complete hydrogen termination. Thus, it is not possible to tunnel from the tip into empty states on the surface.

Results

Oxidized Si(111). Figure 1a shows single atomic steps on a clean oxidized Si(111) surface imaged with tapping mode AFM. However, although we generate −66 dBm of third harmonic signal on this surface, and can use AC feedback to maintain a very stable, low noise junction, we are unable to generate AC images with high resolution of surface features. Figure 1b shows a typical AC image on this surface. Although these two images are taken on different spots on the surface, there should be similar features in both images. However, none of the observed structures in the AC images can be ascribed to known topographic features. However, since some images produce a larger quantity of smaller repeatable features than others, it appears that the resolution on this surface is determined by the tip radius and tip−sample separation, as one would expect for imaging via third harmonic signal produced by capacitive nonlinearities.

H−Si(111). Figure 2a,b shows simultaneous DC and AC images of H−Si(111) taken under DC feedback. Although the AC image shown here is strongly correlated to the DC image, AC image quality varies a great deal. The typical third harmonic signal is −66 dBm, which can be used for both imaging and feedback control. The tunneling current and surface DOS vs voltage shown in Figure 2c,d show striking nonlinearities as a function of the applied voltage.

Even though we generate more than enough third harmonic signal on H−Si(111), using the microscope in AC feedback mode is not as straightforward as on other samples. When operated with the DC bias set to 0 V, we observe a strong third harmonic signal (around −67 dBm) but produce images that are completely flat with no discernible features. However, if the DC bias is set to 1.5 V, we generate images that look like Figure 3a, showing atomic resolution in the *z* direction. These images show triangular features characteristic of the Si(111) surface, as well as single atomic steps. Furthermore, Figure 3b shows a plot of the tunneling current (black circles) and third harmonic signal (gray squares) as a function of the distance between the tip and the sample. Both curves show roughly the same exponential dependence on the tip−sample separation. However, since these data were taken within the DC tunneling range using DC feedback control, they does not extend out far enough to rule out capacitive AC signals.

Molybdenite (MoS_2). MoS_2 generates a large third harmonic signal for all tested DC biases between 100 mV and 2 V and tunneling currents between 0.5 nA and 2 nA. The typical third harmonic signal is −62 dBm. Figure 4a,b shows simultaneous DC and AC images taken with DC feedback controlling the distance between tip and sample. Although none of the observed details can be assigned to topographic features, the AC images show the same features as DC images, as would be expected if the third harmonic signal were exponentially dependent on the tip−sample separation. However, although we can get atomic resolution (albeit noisy) with the DC signal in DC mode, we have thus far been unable to achieve atomic resolution in AC images, regardless of which signal is used for feedback. One additional observation that supports the possibility of producing third harmonics through tunneling mechanisms is that the measured tunneling current vs voltage curve for MoS_2 demonstrates a significantly nonlinear relationship, as shown in Figure 4c. Figure 4d shows the DOS, which varies widely with energy.

Covellite (CuS). Figure 5a,b shows simultaneous DC and AC images taken with DC feedback. Line scans taken through the DC image yield a single step height of 4.7 Å and a double step height of 8.2 Å, which correlate well with a single and

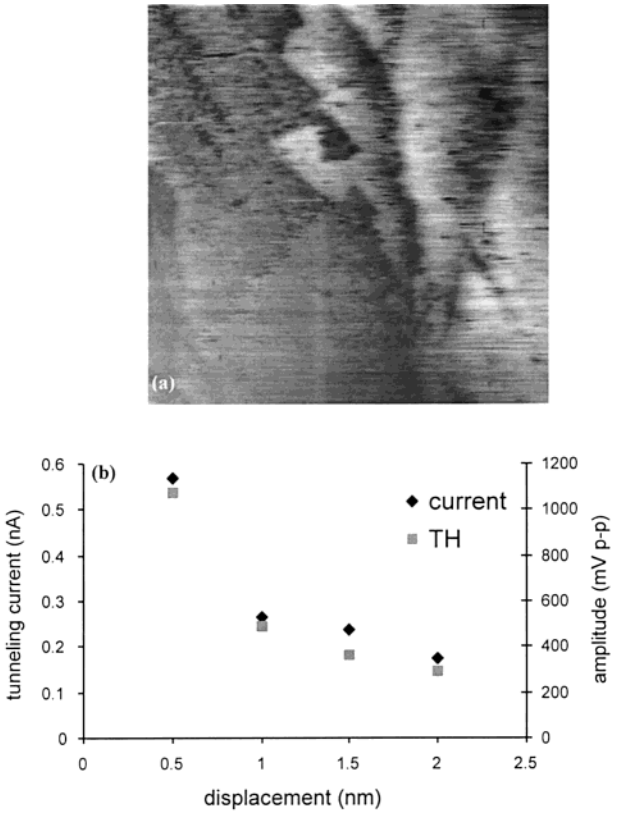

Figure 3. (a) 300 nm × 300 nm AC−STM height image of H−Si(111), taken with AC feedback. AC bias 1.29 V_{p-p}. Scale, black to white 0 to 8.66 nm. (b) Signal strength vs tip−sample separation on H−Si(111). Data plotted as displacement from DC feedback position, using 1.5 V bias and 1 nA tunneling current.

double CuS bilayer.[11] Although the steps are clearly visible in the DC image, they are very difficult to see in the AC image. This is due to the very small third harmonic signal measured on this surface. Since the typical signal is −74 dBm, just 2 dBm above the noise floor, only very large features such as bilayers or multiple steps are visible in the image. Furthermore, this is not enough third harmonic signal to operate in AC feedback mode. Figure 5c,d shows the measured tunneling current vs applied bias and DOS for this sample. The *I*/*V* curve is surprisingly linear, given that CuS is considered to be a semiconductor.

Galena (PbS). Figure 6a,b shows simultaneous DC and AC images taken under DC feedback control. Since both images show atomic resolution in the *z* direction, it seems likely that the AC signal is produced mostly via nonlinearities in the tunneling current. This observation is well supported by the current vs voltage curve and the surface DOS for PbS, shown in Figure 6c,d. As with MoS_2, we demonstrate both an energy-dependent DOS and a large third harmonic signal. The typical third harmonic signal is around −66 dBm. This is more than enough signal for both AC imaging and AC feedback. The measured step heights are approximately 3.2 Å for both DC STM and AC−STM constant signal images.

Although galena is known to oxidize slowly in air[12] (and even more slowly in the controlled glovebox environment), we were able to induce oxidation using the STM tip. By scanning over the same area, we were able to completely oxidize this region of the surface in a few hours. Figure 7 shows selected images from this "time-lapse" AC−STM, covering the time period from clean PbS (7a) to 2 h after the start of scanning (7l).

In image 7a, there are only a few dark patches, covering less than 10% of the surface, and these seem to be associated with

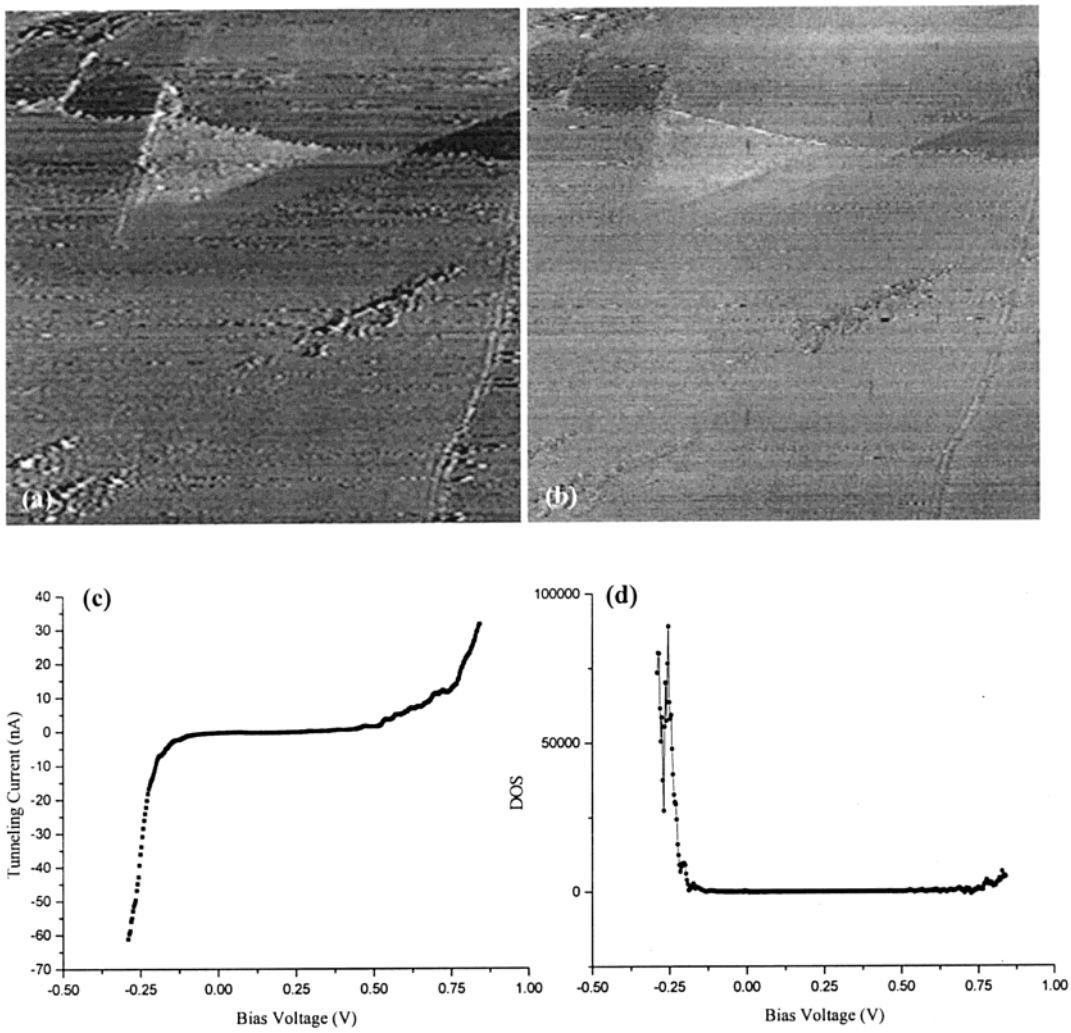

Figure 4. 300 nm × 300 nm MoS_2 images. (a) DC height image. Scale, black to white 0 to 7.22 nm. (b) TH image under DC feedback. DC Bias −1 V, current 1 nA, AC bias 1.29 V_{p-p}. (c) Tunneling current and (d) DOS vs applied bias on MoS_2.

step edges. The depth of the lighter patches (as in the patch marked A) is ∼5.9 Å, while the depth of the darker patches (as in the patch marked B) is ∼12.1 Å. This is equivalent to two or four atomic layers, respectively. Most of the observed patches are ∼5.9 Å deep. In image 7b, there are many more dark patches, and not all of them are associated with visible defects such as steps (considering that we cannot see single-atom defects at all). In addition, the patches in image 7b are noticeably larger than those in image 7a−for example the patch marked C in both images. However, although the patches have increased in size laterally, they do not become any deeper, indicating that the reaction is confined to the surface at this point. On image 7b the oxidation patches cover approximately 22% of the surface, more than double the area from the previous image.

By image 7c, taken 25 min into the reaction, the patches are both noticeably larger and are starting to coalesce. Oxidation patches dominate the image, although the step structure is faintly visible underneath. On the left side of the image, there are considerably fewer oxidation patches, and there is also some step structure on the very edge. Immediately prior to taking this image, the tip was moved to a new position to ensure that the tip was still sharp enough to resolve steps on an unoxidized portion of the sample. When the piezo was moved back to the original location, there was a positioning error due to thermal drift and piezo hysteresis, pushing the imaging area to the right and exposing virgin galena on the far left. For orientation, the patch C is once again labeled, this time in the far right corner of the image. This identification is made by comparing the pattern of patches in the two images. Patch D is also labeled to aid in orientation, allowing for piezo drift over the course of the experiment. By image 7d, 35 min into the experiment, there are no new oxidation patches, but the existing patches are much larger and still coalescing.

At this point, the patches seem to stop growing. For the next three images in the sequence (about 15 min, images not shown), no significant changes occur from one image to the next. Finally, in image 7e, a different type of oxidation patch starts to appear, especially at the bottom of the image. These new patches appear to orient along step edges and are only 2.9 Å deep, which corresponds to one atomic layer. Once this new type of reaction begins, it rapidly dominates the surface topography, expanding from the narrow lines to fill more of the surface, as seen in image 7f, which is taken 10 min after image 7e. In addition, for the first time, the round oxidation patches of the previous discussion appear to be shrinking in radius, as if they are being filled in.

In the next image, 65 min after the start of the experiment and 5 min after image 7e, the shallow oxidation region extends over most of the surface, and the deep circular oxidation patches are almost gone. Images 7f and 7g, which show every other image in the sequence (10 min between images) show an increased tendency toward order. The patches can clearly be separated into layers, although the rectangular step structure of the clean galena surface is lost. The measured height difference

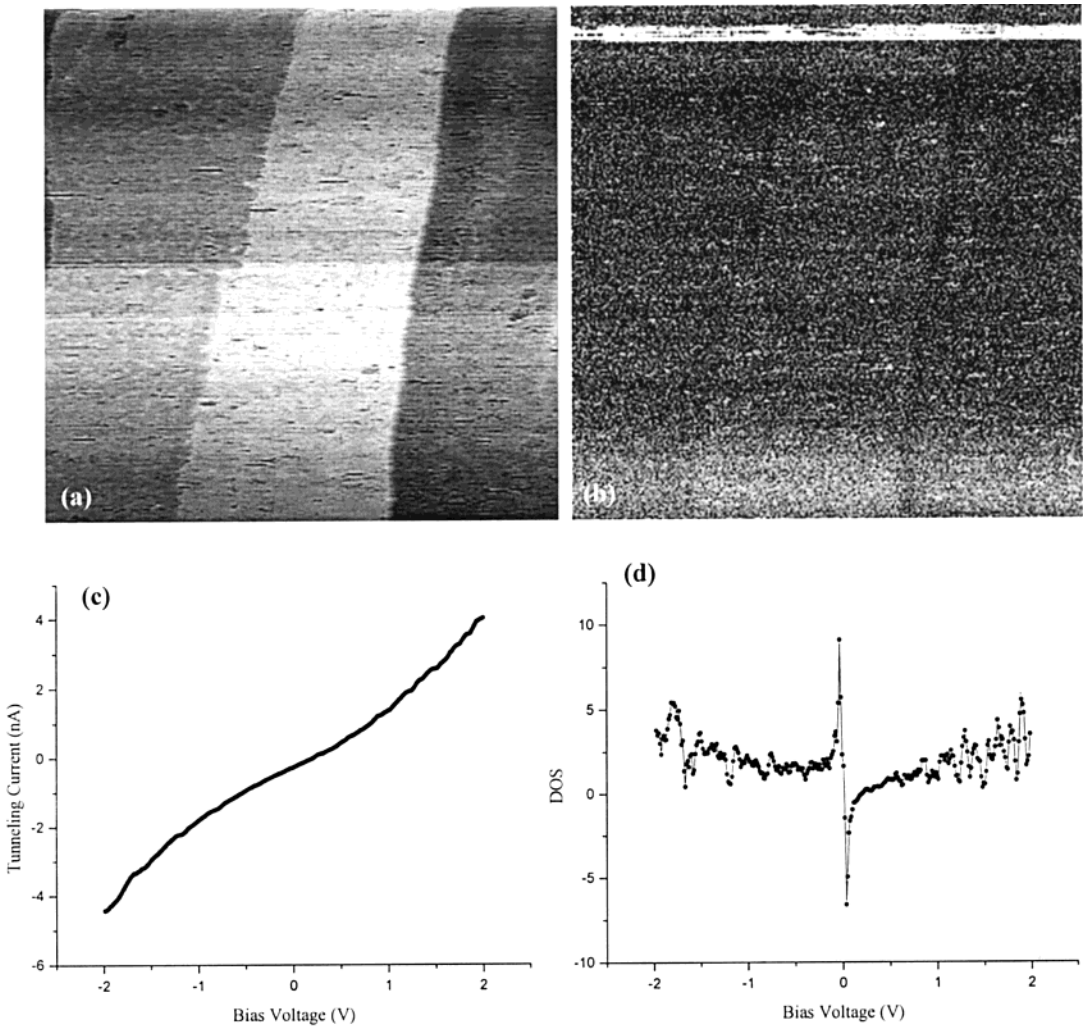

Figure 5. 300 nm × 300 nm (a) DC height image and (b) TH signal image of CuS, taken with DC feedback. $I_t = 0.2$ nA, DC bias = −1 V. AC bias = 1.29 V_{p-p}. Left scale, black to white, 0 to 5.28 nm. Right scale, black to white, 0 to 0.27 V. (c) Tunneling current and (d) DOS vs applied bias for CuS. In the DOS plot, the large peaks around 0 V are artifacts introduced by the inflection point in the *I*/*V* curve, then plotted as (d*I*/d*V*)/(*I*/*V*).

between the layers is 3.2 Å, which correlates well with 2.97 Å, the height of a single atomic layer. In the final row of images, 7j through 7l, the new layer covers most of the 300 × 300 nm^2 area, although some "seams" are visible where the patches did not completely coalesce. In addition, several new round oxidation patches have begun to grow that are similar in appearance and depth to those appearing in image 7a.

Discussion

Silicon. As in previous studies, the evidence from Figure 1a,b suggests that for oxidized silicon, the third harmonic signal arises from a capacitive rather than a tunneling mechanism. Since a capacitive signal will decay as 1/*d*, where *d* is the tip−sample separation, rather than exponentially, the AC−STM does not provide atomic-level resolution on this surface. However, it is possible to image this insulating surface to demonstrate features that are repeatable from scan to scan. These features probably correspond to different electronic, rather than topographic features. Local variations in the surface capacitance due to defects at the silicon−silicon oxide interface or variations in the carrier density may give rise to the observed features.

Although hydrogen-terminated silicon has never been studied with the AC−STM before, Seifert's explanation of signal generation on a semiconductor surface through a capacitive mechanism would be expected to apply.[3] However, we observe a much more complex behavior. Figure 3b shows a measurement of the third harmonic signal and the tunneling current as a function of the change in tip−sample separation. Both of these signals show an exponential decay as the tip moves away from the sample. This indicates a tunneling mechanism for the generation of higher harmonic signals.

Furthermore, although we can measure and use the third harmonic signal for feedback at any applied DC bias, we can only image atomic steps with an applied DC bias larger than 1.5 V. Previous work with the AC−STM has shown that the strength of the third harmonic signal can depend on the applied DC bias at the same nominal tip−sample separation on graphite[4] and oxidized silicon.[7] If the magnitude of the third harmonic signal is strongly affected by the applied DC bias, then we may be measuring two different "kinds" of third harmonic signal on H−Si(111), by analogy with CuO. On CuO, measurements of the third harmonic signal as a function of the tip−sample separation show two distinct regions. Outside the DC tunneling range there is a small third harmonic signal that slowly rises as the tip approaches the sample. Once the tip reaches the DC tunneling range, however, there is a sharp increase in the third harmonic signal that rapidly increases until the tip crashes into the sample.[2] Kochanski assigned the third harmonic signal

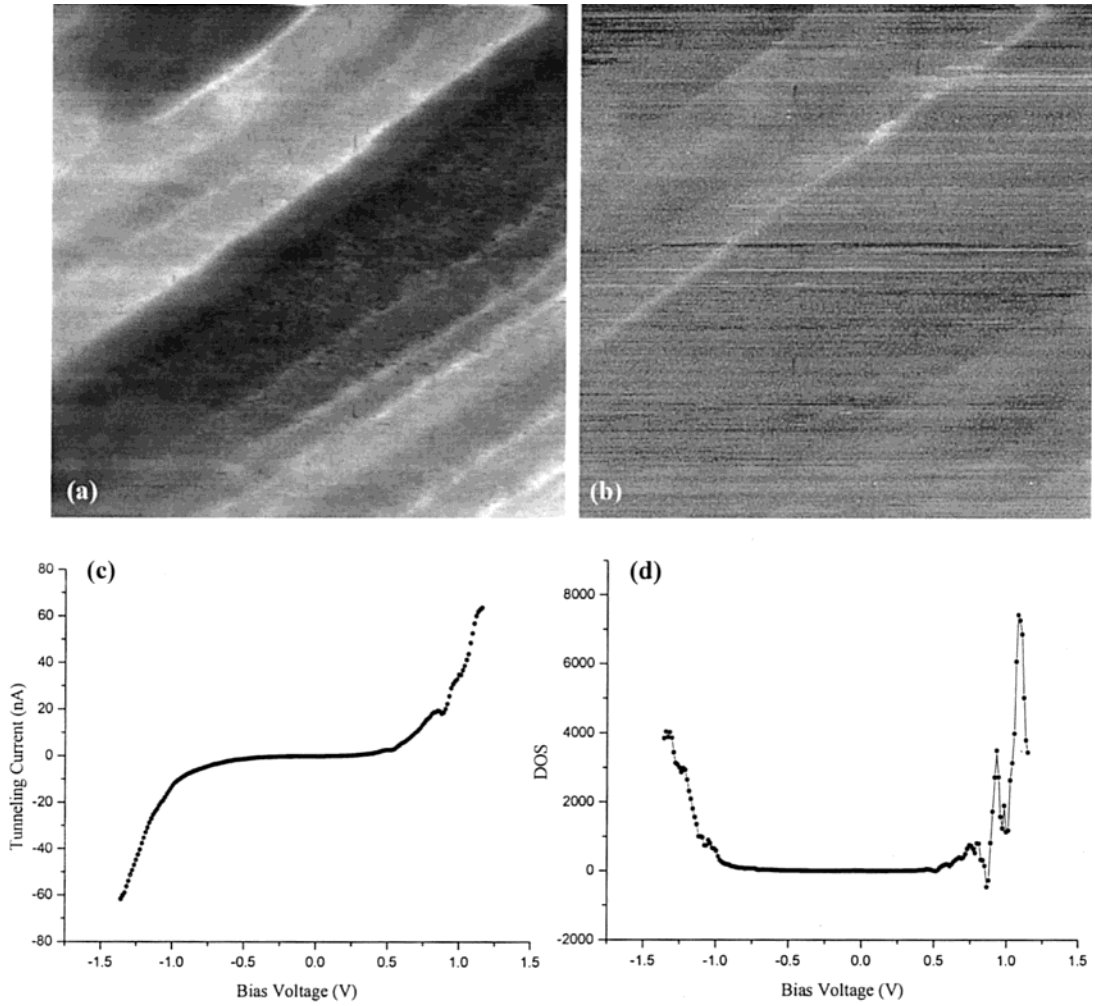

Figure 6. 300 nm × 300 nm images of PbS, taken with DC feedback. (a) DC height image. Scale black to white 0 to 7.40 nm. (b) TH signal image. DC bias 200 mV, $I_t = 1$ nA, AC bias = 1.29 V_{p-p}. (c) Tunneling current and (d) DOS vs applied bias on PbS.

produced outside the tunneling range to capacitive effects. The third harmonic signal within the DC tunneling range was assigned to AC tunneling effects.[2]

Thus, the reason we need to maintain the DC bias at 1.5 V to produce images under AC feedback is due to the dependence of the third harmonic signal on the applied bias. Since we generate more third harmonic signal when the bias is at 0 V than when the bias is at 1.5 V, the tip−sample separation is larger at 0 V than at 1.5 V. Thus, at 0 V, the majority of the third harmonic signal is produced by capacitive nonlinearities, producing a large signal with little contrast. At 1.5 V, the tip−sample separation is smaller, so AC tunneling, which depends exponentially on the tip−sample separation, produces the majority of the third harmonic signal. Therefore, at this bias, we can image the surface with atomic resolution in the *z* direction, as shown in Figure 3a.

Sulfides. Although we were unable to achieve atomic resolution with MoS_2 using the AC−STM in either mode, there is some evidence that AC tunneling provides the majority of the third harmonic signal measured on this sample. Under experimental conditions, the AC−STM sweeps the Fermi level of the tip with respect to the sample. Thus, different local densities of states are probed, depending on the total magnitude of the AC and DC biases. Figure 4c,d shows that the *I*/*V* curve (and thus the local DOS, since the STM current is proportional to the DOS at the surface)[10] provides ample nonlinearity for the generation of higher harmonics through tunneling pathways. Although none of this evidence is conclusive proof of a dominant tunneling nonlinearity, one final observation in support of this hypothesis is that there is no measurable third harmonic signal on MoS_2 when the tip is not within DC tunneling range of the sample. This strongly implies that capacitive effects are not important on this sample, because if the capacitive mechanism were dominant, we would expect to see a third harmonic signal while near, but not within, DC tunneling range.

On CuS, there is not enough AC signal produced to allow AC feedback. Without strong evidence from images, it is difficult to determine the source of the nonlinear signal in CuS. However, the presence of step edges, albeit faint ones, is suggestive of an exponential relationship between gap height and third harmonic signal, similar to the other studied sulfides. Furthermore, the measured tunneling current vs applied bias is surprisingly linear for this sample, as seen in Figure 5c. Figure 5d shows the DOS. There is an artifact of calculation produced by the inflection point in the *I*/*V* curve near 0 V, but other than that, the DOS is fairly flat and uniform. In addition, there appears to be no band gap in the DOS for this material, even though the reported bulk band gap is ∼1 eV.[11] Supporting this observation, other researchers have noted that CuS often behaves more like a metal than a semiconductor, in terms of its resistivity and other electronic properties.[11] Although this is not fully conclusive evidence, the strong correlation between a DOS that depends more or less linearly on the bias voltage and a very small third harmonic signal is suggestive of a tunneling third

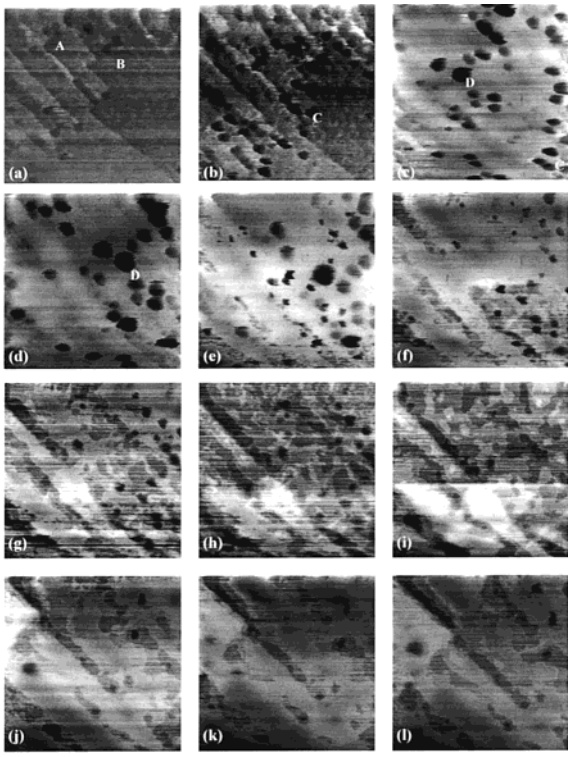

Figure 7. "Time lapse" AC−STM images. AC bias = 1.29 V_{p-p}, AC setpoint = −61 dBm. (a) 5 min, (b) 10 min, (c) 25 min, (d) 35 min, (e) 50 min, (f) 60 min, (g) 65 min, (h) 70 min, (i) 80 min, (j) 100 min, (k) 110 min, (l) 120 min. Initial reaction shown in (a) through (d). Second reaction begin in (d) and (e). First layer "complete" in (j). Next layer begins reacting in (k) and (l).

harmonic generation mechanism. In addition, as with the other sulfides, no AC signal is observed when the tip is out of tunneling range but near the sample.

Galena (PbS). Similar to the other sulfides studied, the third harmonic signal appears to arise from nonlinear tunneling effects. The strongest evidence for this is that the measured step heights are the same for both types of signal, providing strong evidence that the third harmonic signal is exponentially dependent on the distance between the tip and sample. Since the energy dependence of the surface DOS is intermediate to that of MoS_2 and CuS, the magnitude of the third harmonic signal should fall between those two, and at −66 dBm, it does.

Although the surface oxidation of galena has been studied with STM in the past, the formation of an insulating overlayer has limited observations to the early stages of the reaction, before the insulator becomes too thick to tunnel through. The first stages of the reaction, shown in images 7a though 7l show patches growing out from nucleation sites that are located both at step edges and on terraces. These results are similar to those of previous studies, which noted that on natural galena oxidation patches nucleated all over the surface, not just at step edges. In that experiment, oxidation patches were induced by exposure to humid air over longer time periods.[13]

By image 7d, 35 min into the experiment, there are no new oxidation patches, but the existing patches are much larger and still coalescing. This indicates that the nucleation of new oxidation patches is the limiting step, since the oxidation reaction continues once all of the likely sites have been nucleated. Furthermore, oxidized areas appear to enhance the reactivity of neighboring sites, since the size of the patches appears to correlate with how much time has passed since growth began. Further evidence for the activation of surface sites is that the dark patches are growing laterally but are not getting any deeper. In fact, in image 7d, all of the patches are 6.3 Å, which corresponds to two atomic layers.

It is not entirely clear why pitting of the surface, rather than the formation of oxide islands, marks the progress of the reaction. Under the experimental conditions, there is no way for material to be carried away from the surface. In addition, there is no evidence of mechanical removal of material by the STM tip (i.e., there is no build-up of material at the edges of the scan window). One possible explanation for this experimental observation is that the newly formed oxide layer is transparent to the AC−STM. There is some precedence for this interpretation from previous work in the field, which suggests that for Si/SiO_2 samples, the third harmonic signal is sensitive to the oxide−silicon interface.[7] If indeed we are imaging the underlying buried interface between oxide and PbS, the reacted areas would appear to be lower in height than the clean surface due to incorporation of PbS into the oxide layer, as they do in our images.

After image 7d, there are no significant changes in the STM images for the next 15 min. However, since we are unable to achieve lateral atomic resolution with the AC−STM under these conditions, it is unclear why the reaction appears to stall for 15 min. One possibility is that the changes that are occurring are on the atomic scale, and we are unable to resolve them. Another possibility is that the reaction occurs in stages, where the second reaction has a significant induction phase.

The second reaction, first seen in image 7e, can be differentiated from the initial reaction by three significant observations. First, the new features of the second reaction are 2.9 Å in height, which corresponds to a single atomic layer. In contrast, the first reaction features seen are 6.1 Å, corresponding to two atomic layers. Second, the new features starting in image 7e appear solely at step edges (or where the steps appeared in the clean galena image). Growth at these sites is significantly faster along the step edges than out from them. This anisotropic behavior is in stark contrast to the first reaction, which occurred both at step edges and on terraces to produce round features indicating an isotropic reaction. Finally, the second reaction occurs much faster than the first one does. It takes 35 min for the first reaction to cover 17% of the surface, while the second reaction does this in 10 min.

This two-reaction interpretation is consistent both with our STM images and with earlier non-STM studies of the galena surface. In previous studies with XPS, exclusively lead-containing products are seen in the early stages of the reaction, with sulfur-containing products appearing later.[14] In addition, previous STM studies have demonstrated that due to geometry consideration on the galena surface, sulfur reactions should occur much faster at step edges than on the terrace, which is consistent with our observations of the second reaction.[15]

Once the second reaction starts, it rapidly proceeds out from the step edges to encompass the whole surface. Simultaneously, the original round patches disappear from the surface. It is unclear why this occurs from the STM images. However, new round patches appear again after the formation of a more or less complete layer, as seen in image 7j, indicating that the oxidation of galena proceeds in a layer-by-layer fashion. At this point, there is no measurable DC tunneling current, although the AC−STM continues to produce images showing single atomic steps.

Conclusions

We were able to use the AC−STM to produce images with atomic resolution in the *z* direction. On CuS, PbS, and H−Si-

(111), AC images taken under DC feedback showed single atomic steps. In addition, on PbS, we were able to demonstrate single atomic steps under AC feedback with no applied DC bias. On H−Si(111), we were also able to generate single atomic steps under AC feedback, but with an applied bias of 1.5 V. From these measurements made on different materials, it is possible to determine the dominant nonlinearity, and thus the likely source of the third harmonic signal. For MoS_2, CuS, and PbS, the resistive pathway seems to dominate. For all of these materials, there was no third harmonic signal produced when the tip was out of DC tunneling range. Furthermore, plots of the energy dependence of the local density of states, as determined from the measured tunneling current vs bias voltage plots, indicate that the strength of the third harmonic signal correlates well with the degree of nonlinearity in these plots.

For H−Si(111), our data is consistent with a "dual mode" mechanism of third harmonic signal generation. When the tip is within tunneling range, AC tunneling can occur, leading to a third harmonic signal that is exponentially dependent on the tip−sample separation. However, when the tip is further from the surface, nonlinearities are generated by capacitive nonlinearities, producing a third harmonic signal that does not allow for high-resolution imaging. From our observations, it appears that in order to know whether the AC−STM will produce high-resolution images of a given surface, it is necessary to try the microscope on the specific surface to determine the mechanism of the third harmonic generation. However, similar classes of materials, such as the layered sulfide semiconductors appear to behave the same way with regard to third harmonic generation.

Using the AC−STM, we were able to follow the oxidation of galena from a clean, freshly cleaved surface to a completely oxidized surface. This represents the first time the AC−STM has been used to study surface reactions that convert a surface from conductive to insulating. With the AC−STM, we are able to monitor the reaction even after there is no measurable DC tunneling current. Thus, we are able to observe structures that more closely resemble those found in real world applications of galena than those observed in previous studies. In the images, it appears that the third harmonic signal is generated only by the galena and not the forming oxide. Thus, the resulting oxide layer is transparent to the AC−STM and the oxidized areas appear as pits or depressions. By using the AC−STM to study surface oxidation, we have demonstrated for the first time that this instrument can monitor the progress of reactions in situ.

Acknowledgment. The authors thank James Gladden and Dr. Colin Mailer for their help in building the microscope, as well as Dr. Bruno Michel and Dr. Paul Weiss for their helpful discussions. The authors also thank Dr. Kevin Rosso (Pacific Northwest National Lab) and Dr. Bernard Evans (University of Washington) for providing sulfide samples. A.S.B. was supported by the University of Washington Center for Nanotechnology.

References and Notes

(1) Wiesendanger, R. *Scanning Probe Microscopy and Spectroscopy*; Cambridge University Press: New York, 1994.
(2) Kochanski, G. P. *Phys. Rev. Lett.* **1989**, *62*, 2285.
(3) Seifert, W.; Gerner, E.; Stachel, M.; Dransfeld, K. *Ultramicroscopy* **1992**, *42*−*44*, 379.
(4) Schmidt, J.; Rapoport, D. H.; Frölich, H.-J. *Rev. Sci. Instrum.* **1999**, *70*, 3377.
(5) Bourgoin, J.-P.; Johnson, M. B.; Michel, B. *Appl. Phys. Lett.* **1994**, *65*, 2045.
(6) Schmidt, J.; Rapoport, D. H.; Behme, G.; Frölich, H.-J. *J. Appl. Phys.* **1999**, *86*, 7094.
(7) Michel, B.; Mizutani, W.; Schierle, R.; Jarosch, A.; Knop, W.; Benedickter, H.; Bächtold, W.; Rohrer, H. *Rev. Sci. Instrum.* **1992**, *63*, 4080.
(8) Johnson, M. B.; Bourgoin, J.-P.; Michel, B. *Microelect. Eng.* **1995**, *27*, 539.
(9) Stranick, S. J.; Weiss, P. S. *J. Phys. Chem.* **1994**, *98*, 1762.
(10) Avouris, P. *J. Phys. Chem.* **1990**, *94*, 2246.
(11) Rosso, K. M.; Hochella, M. F., Jr. *Surf. Sci.* **1999**, *423*, 364.
(12) Nowak, P.; Laajalehto, K. *Appl. Surf. Sci.* **2000**, *157*, 101.
(13) Kim, B. S.; Hayes, R. A.; Prestidge, C. A.; Ralston, J.; Smart, R. St. C. *Appl. Surf. Sci.* **1994**, *78*, 385.
(14) Nowak, P.; Laajalehto, K.; Kartio, I. *Colloids Surf. A* **2000**, *161*, 447.
(15) Eggleston, C. M.; Hochella, M. F. In *Environmental Geochemistry of Sulfide Oxidation*; Alpers, C. N., Blowes, D. W., Eds.; American Chemical Society: Washington, DC, 1994.